Median Energy Imaging of Supernova Remnants with Chandra X-ray Observatory

A thesis submitted in partial fulfillment of the requirement for the degree of Bachelor of Science with Honors in Physics from the College of William and Mary in Virginia,

by

Anne E. Blackwell

Accepted for Honors
(Honors or no-Honors)

Advisor: Prof. Seth Aubin

Prof. Marc Sher

Prof. Christopher Bailey

External Research Advisors:

Dr. Daniel Castro
Center for Astrophysics | Harvard Smithsonian

Dr. Rodolfo Montez Jr.
Center for Astrophysics | Harvard Smithsonian

Williamsburg, Virginia
May 2019

Contents

Acknowledgments

I would like to thank my research advisors Dr. Rodolfo Montez Jr. and Dr. Daniel Castro for starting and continuing this project me. Without their endless support and encouragement in all forms, this research would not have been possible. I would also like to thank Dr. Seth Aubin for encouraging me to pursue this research and his support at William & Mary. Many thanks to family, friends, and peers for endless reassurance, help and optimism.

List of Figures

List of Tables

Abstract

Supernova remnants (SNRs) play an important role in shaping the energy density, chemical enrichment, and interstellar medium (ISM) of galaxies, and in our understanding of stellar evolution. Due to the high plasma temperatures of SNRs, they primarily emit X-rays. Using data collected with the Chandra observatory, we study a novel statistical imaging analysis technique to probe the underlying structure and physical properties of DEM L71, a SNR in the Large Magellanic Cloud. We used the statistical properties of the photons within an image pixel, such as the median energy, to make images of the energetics across the SNR. Based on the spatially-resolved statistical information we identified an unexpected feature. We present the analysis of the spectra, (column density N_H , plasma temperature kT, and ionization timescale τ) of this feature and DEM L71 and surrounding regions. We conclude that this feature has a higher abundance of ejecta material than surrounding regions. Spectra fits give a ratio of the energy flux normalization values of the ejecta model to the ISM model as .32 for the region of interest (region 2). This value is twice as much as any of the regions of extracted spectra surrounding Region 2. This study demonstrates the utility of the median energy imaging technique to identify new energy structures of SNRs.

Chapter 1

Introduction

Supernova remnants (SNRs) play an important role in shaping the energy density, chemical enrichment, and evolution of galaxies. A SNR is the result of a supernova explosion, the dramatic death of the largest stars and some of the most powerful explosions in the universe. The shocks of a SNR compress and heat the surrounding medium and accelerate particles to cosmic ray (CR) energies. In addition, the ejecta from supernovae seed the galaxies with heavy elements (carbon, oxygen, neon, iron, and higher atomic numbers) and the resulting elemental distribution and patterns can be used as clues to understand the nature of the supernova progenitors. Studies of supernova remnants help us understand how stars evolve and collapse, how the shocks from the supernova explosions distribute energy in their host galaxies, and how the explosions enrich the environment for subsequent generations of stars and their planets. Thus, the study of SNRs allows for understanding issues of broad relevance in astrophysics. This project makes use of a novel statistical imagining analysis technique that probes the underlying structure and physical properties of these remnants. The statistical imagining analysis was researched over the summer of 2018. With the use of this technique, we have found a new energetic structure in the first SNR to which we have applied this approach. This semester, we have been analyzing the spectra of this energetic structure and surrounding regions, to identify

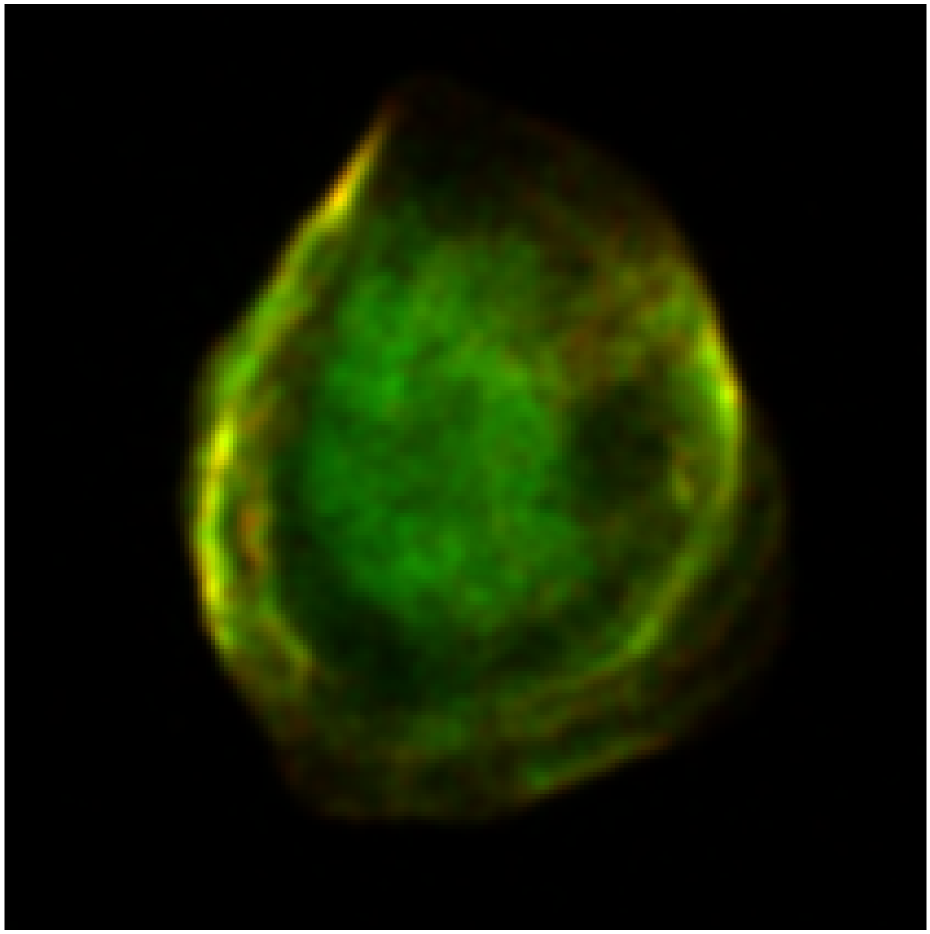

Figure 1.1: X-ray image of SNR DEM L71 located in the LMC. This is a rgb image with specific energies associated with each of the three images. The energies are: 200-700 eV (red), 700-1100 eV (green), and 1100-2600 eV (blue)

its physical origin. With this study we hope to further understand the behavior of SNRs, in particular the energetic structure discovered in DEM L71, a SNR located in the Large Magellanic Cloud (see Figure 1.1).

This thesis is organized in the following manner. Chapter 2 describes all previous work done over the summer of 2018 that has led to this honors thesis project. In Chapter 3 we discuss theory including the timescale parameters and plasma models. Research methods are covered in Chapter 4 and Chapter 5 contains the results. We conclude with Chapter 6 and present on the outlook for future work.

Chapter 2

Background: The Remnants of Supernova Explosions

Supernova remnants are the result of the interaction between the material ejected in supernova explosions and the surrounding media. Supernova explosions come in two flavors, Type Ia and core-collapse supernovae. Type Ia supernovae are thermonuclear explosions, and they are the result of accretion from a non-degenerate star onto a white dwarf or from the merger of two white dwarfs. In either scenario, quantum degeneracy pressure in the white dwarf becomes insufficient to balance gravitational self-attraction and the star collapses. Type Ia supernovae leave behind no compact remnants (neither a black hole nor a neutron star), and all of the mass from the progenitor is ejected outward during the explosion.

Core collapse supernovae take place in an altogether different way. Massive stars (with a mass approximately eight times larger than that of the Sun) end their lives in a rapid gravitational collapse and a subsequent violent explosion. The collapse is triggered when the heat produced through nuclear fusion in the inner most regions of these stars decreases past the threshold where hydrostatic pressure can no longer counteract gravitational forces. Immediately after the core collapses, neutron degeneracy pressure stops the further implosion of material creating a rebound of the implosion, an explosion and outward-moving shock wave which is characteristic of both types of supernova explosions. The subsequent explosion expels the outer layers of stellar material outwards, but the inner core of the stellar progenitor is left behind as a neutron star or black hole.

Once the explosion (Type Ia or core-collapse) occurs, a shock wave moves outward from the progenitor and plows into the uniform interstellar medium (ISM), or the circumstellar material (CSM) if the stellar progenitor had substantially modified the surrounding material through late-phase stellar winds. This "forward shock" sweeps up material in the ISM/CSM compressing the material and heating it to temperatures on the order of million degrees Kelvin. This shock-heating produces thermal emission in the X-ray band [1]. As the forward moving shock runs into the ISM/CSM material, the resulting deceleration of the ejecta produces a reverse shock that travels inwards relative to the outer blast wave, compressing and heating the supernova ejecta. Figure 2.1 shows a diagram of the profile of a SNR and its surroundings. At the forward shock, particles (both ions and electrons) are accelerated to relativistic speeds through diffusive shock acceleration, resulting in non-thermal emission [2]. As a result of interactions between these relativistic electrons with local, shock-compressed ISM/CSM and possibly amplified magnetic fields, synchrotron radiation may be generated.

After the initial evolution phase of the SNR, when the shock dynamics and emission are dominated by the expanding ejecta, the swept up ISM/CSM mass becomes larger than the total ejecta mass and the SNR reaches the adiabatic expansion or Sedov-Taylor phase [1]. During this phase, adiabatic expansion causes the cooling of the material, while radiative cooling is relatively insignificant [1]. Immediately after the Sedov-Taylor phase comes the radiative, or "snow plough", phase in which the energy losses due to radiation become dynamically significant. During this time the evolution of the shock radius can be described best using conservation of momentum [1]. Finally, the temperature and shock velocity of the shock wave becomes comparable to the temperature and movement of the interstellar medium, and the SNR is considered to have dispersed into the ISM.

These are the general phases that all SNRs go through as they explode, expand, and cool. However, the structure of each SNR and the abundance of different elements in each one depends on the progenitor star and the nature of the surrounding material. Additionally, different regions of a SNR may be in different phases at the same point in time. Thus, we can apply this general structure to the overall development of the SNR but many key underlying details and features such as a non-spherical ejecta shell, lobes, knobs, or tendrils of ejecta must be further studied to be fully understood.

The X-ray band represents an ideal window into thermal and non-thermal emission in SNRs, providing a unique way of constraining the distribution, conditions, and composition of both the shocked ejecta and either the ISM or the CSM, as well as the non-linear particle acceleration process.

2.1 Previous Work

The current senior thesis research builds on research started this past summer through a NSF funded REU program at the Maria Mitchell Observatory, Nantucket MA. During the summer, I studied a novel statistical approach to astrophysical X-ray imaging. This technique utilizes the statistical capabilities enabled by the nature of Chandra X-ray observations and its spatial imaging power to produce new data products based on the energy quartiles of collected photons.

The technique involves studying the photon energy characteristics on a pixel by pixel basis to study the spatial variations in a SNR. Energy quartile images are visual depictions of the energy information for X-ray photons detected from the SNR. The three quartiles include 25%, 50%, and 75% percentiles of the ensemble of X-ray photon energies in each pixel of the X-ray observation. Specifically, 50% percentile is also

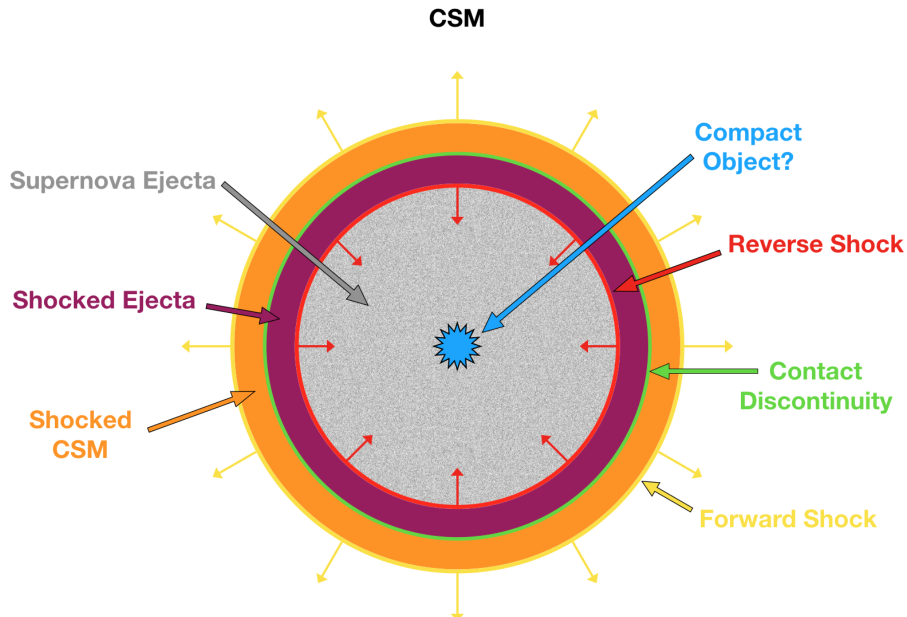

Figure 2.1: "Onion" diagram of a SNR. This shows a cross-section of a SNR. In the center is a compact object (blue), that will only be present in core-collapse supernovae, followed by the supernova ejecta (grey) - material produced by the supernova, which cools efficiently through adiabatic expansion. As the initial forward shock (FS, yellow) interacts with the ISM/CSM, it loses velocity producing a reverse shock (RS, red) that travels inwards relative to the FS. Both FS and RS shock the material they interact with and create shells of hot dense X-ray emitting gas, respectively. Shocked ISM/CSM by the forward shock is shown in orange, and ejecta shocked by the RS is shown in purple. The boundary separating these two shocked regions is known as the contact discontinuity (CD, green).

known as the median value, in this case, the median energy. The median energy is obtained by finding the median, or middle, energy of all of the photons in a single pixel listed in numerical order by energy. The 25% and 75% quartiles can be found using the same method except identifying the first quarter value and the third quarter value in the energies of all the pixels individually. A similar, but not exactly the same, technique has been applied to point sources by others, but not as images nor to SNRs [3]. We perform this operation on every pixel to obtain the median energy image.

Pixels from the SNR provide a strong signal with higher photon counts, but pixels

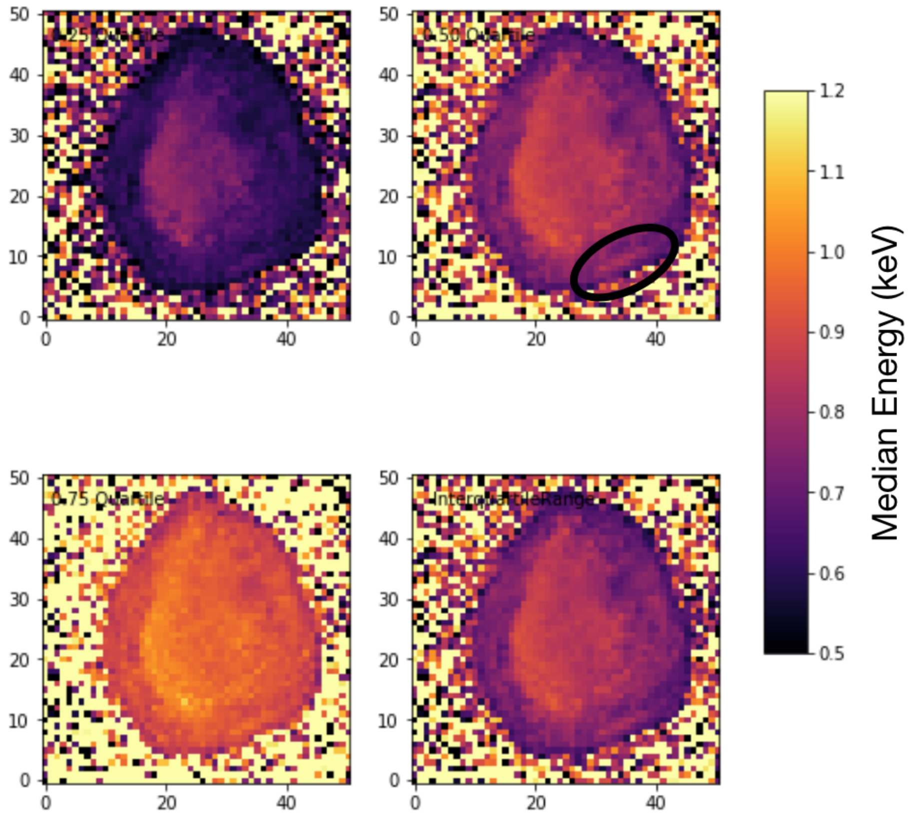

Figure 2.2: Quartile image of SNR DEM L71 located in the Large Magellanic Cloud. The four quartile depicted are 0.25 (top left), 0.5 (top right), 0.75 (bottom left), and the interquartile range 0.75-0.25 (bottom right). Each quartile represents a specific energy level defined by the distribution of energies listed in numerical order. Using this distribution, the median energy (0.5 quartile) is the median of the photon energies listed, 0.25 is the first quarter value and 0.75 is the third quarter energy value.

from the background contain a very small number of photons whose energy varies greatly, the noise, making the median energy look random in the background. For example, using this method we identified an interesting new structure in SNR DEM L71 located in the Large Magellanic Cloud (see Figure 2.2). This structure can be seen in the bottom right of the lighter outer oval (outward-moving shockwave) as a dark band of higher median energy pixels. A more detailed image of the identified structure can be seen in Figure 2.3. Here the structure is highlighted by an energy

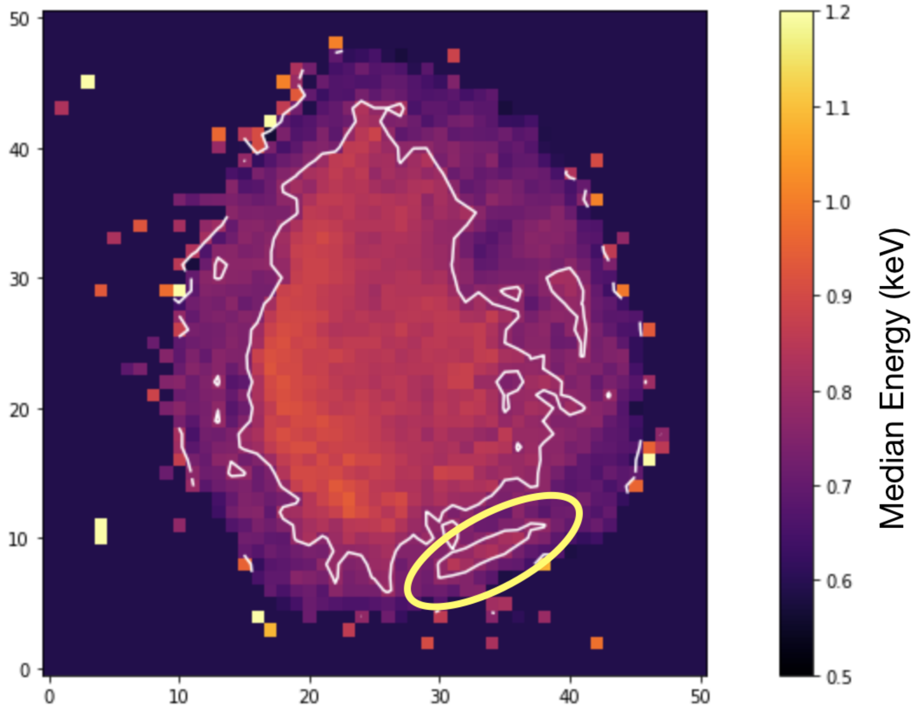

Figure 2.3: Contour image of the median energy plot of DEM L71. The contour shown represents an energy of 750 eV. The area of interest, the high energy structure is circled by the yellow oval and a contour just inside the southeast edge of the SNR and can be seen as a dark red against the purple.

contour at 750 eV.

All of this analysis was done using extensive Python 3 coding as well as data reduction using CIAO. CIAO is a program designed specifically for Chandra data analysis. Using Sherpa, a spectral analysis program also designed specifically for Chandra data analysis, we are able to then extract the spectra from regions identified using median energy analysis.

Figure 4.1 and onwards, and associated sections, represents work done during the 2018 Fall and 2019 Spring semesters as work for my senior honors thesis.

2.2 Chandra X-ray Observatory

Chandra is a space-based observatory studying the X-ray emission from some of the most energetic regions of the Universe. An artist's representation of Chandra is show in Figure 2.4. The observatory is monitored and directed from a control center operated by the Smithsonian Astrophysical Observatory (SAO) located at the Center for Astrophysics | Harvard & Smithsonian (CfA) in Cambridge, Massachusetts. X-ray photons are detected as Chandra reflects them through its 30 foot optical bench at the end of which are the science instruments. These instruments work by reacting with the X-ray photons that are focused by the high resolution mirror assembly (HRMA) onto their detectors. The HRMA can focus X-ray photons to high precision on the detector plane, allowing for the sub-arcsecond resolution on the sky. The two instruments are the Advanced CCD Imaging Spectrometer (ACIS) and the High Resolution Camera (HRC), each of which have two different detectors. ACIS uses charged coupled device (CCD) technology while the HRC is a micro-channel plate instrument. These instruments work by reacting with the X-ray photons that are focused by the high resolution mirror assembly (HRMA) onto the detectors. In ACIS, X-ray photons liberate electrons from the silicon detector which are read out by the detector electronics. Higher energy X-rays will liberate more electrons and lower energy X-rays will liberate fewer. With this technique, individual X-ray photons can be detected and their energies can be measured by counting the number of electrons. Thus, each photon comes with an energy, position, and time measurement. Over the course of an observation, all of this data is stored into a data product called an event list. The wealth of information the instruments provide allows us to characterize the spatial, spectral and temporal characteristics of the data.

To generate a count image from the event list, the photons within a given pixel

Figure 2.4: Artist's conception of the Chandra X-ray Observatory. Taken from the Chandra X-ray Center (CXC).

boundary are counted. Since each pixel has a set number of X-ray photons with specific photon energies, you filter the photons to generate narrow energy ranges. For example, Figure 1.1, shows a 3-color image of the SNR DEML 71 which was created by combining three such narrow energy filter images. Because of the low background, even with only a few photons per pixel, we can produce informative images from the event lists. For one year after the data is taken by Chandra, it is exclusively proprietary access to the original principal investigator. After that year, all data is publicly available and stored in an online database. This is the database from which we retreive our data.

Chapter 3

Theory: Timescale Parameters

As broadly discussed earlier, there are many parameters that contribute to the morphological characteristics of a SNR including ISM/CSM density and the type of explosion. Additional details that determine the resulting shape and composition of the SNR including the plasma temperature, kT, ionization timescale τ, and column density N_H. Due to the influence of all three of these parameters on a SNR, their values can be extrapolated from the fit of an extracted spectrum.

In order to better understand the interaction of these parameters with each other, consider the region just inside the forward shock (the outer edge) of a SNR. Here the ISM/CSM has been swept up and recently shocked by the forward shock. The forward shock heats the swept up ISM and CSM to temperatures on the scale of millions of degrees Kelvin. The thermal energy of the plasma can be correlated to the kinetic energy of the particles. This is useful when looking at the energy of individual particles, as the population of the particles in the plasma have different masses. Protons are heavier than the electrons, so they gain more energy and are hotter than the electrons. After the initial shock, more collisions occur in the plasma. Some of the proton and atoms collisions may result in the ionization of the atom. The rate at which protons ionize an atom is called the ionization rate. During this phase of unequal thermal energy distribution among the different particle populations in the plasma, the SNR is in non-equilibrium ionization. A SNR is typically in non-equilibrium ionization due to its low density which makes ionizing collisions occur at a less frequent rate [1]. We are able to look at the state of ionization of the plasma and relate it to a plasma temperature kT. As the ionization timescale τ increases, the temperature throughout the plasma becomes more evenly distributed among the protons, electrons and ions. This means higher energy ions (Ca, Fe and Ni) have had the time to be ionized, and we begin to see stronger emission lines from these higher energy elements in the spectra. Eventually, all of the thermal energy will become equally dispersed throughout the different particle populations in the plasma and complete temperature equilibration occurs [1]. As mentioned earlier, the conditions across a SNR are unlikely to stay constant making it very likely to find multiple τ and kT values in a single SNR.

The column density N_H is independent from τ and kT and has a different effect on the X-ray photons. As the X-ray photons are emitted from the SNR and travel to the observer, they pass through CSM and ISM. This material in the path of the X-ray photons absorbs some of the X-ray photons. In the case of DEM L71, the photons must pass through material in the LMC and the Milky Way. We see the absorption of the X-ray photons in the spectra extracted from the SNR. The amount of material can be determined by studying the absorption via the column density.

All three of these values (kT, τ and N_H) may be obtained for a specified region of a SNR by extracting and fitting spectra.

3.1 Spectral Models

Spectral models are libraries of calculations and assumptions applied to fit an extracted spectrum. We need two different type of spectral models in order to properly fit the SNR spectra: absorption and emission models. Absorption models account for the interaction of the X-ray photons with the ISM and are dictated by the N_H parameter. Emission models the plasma conditions of the designated region and which elements are heated and ionized. By properly fitting models to spectra extracted from the SNR, we are able to gather and study each of the parameters and better understand the behavior of the SNR.

For model fitting and manipulation we use CIAO and Sherpa, two analysis programs developed specifically for Chandra data. In Sherpa, there are pre-made absorption and emission models that can be applied to the SNR. Each of the models deals with different assumptions made about the SNR: whether it is in non-equilibrium ionization, if the plasma has reached equilibrium, the type of absorption the X-ray photons may be experiencing, if the plasma varies greatly in temperature, etc.. Many models may be used at a single time to account for additional variations.

In the case of the absorption models, we have chosen *phabs*, photo-electric absorption of the X-ray photons. Photo-electric absorption occurs when an X-ray ionizes an ion and is completely absorbed, and an electron is released. The model *tbabs* is similar to *phabs* and may also be used for fitting the spectra. The *tbabs* model calculates the absorption of X-rays by the ISM, and differs from *phabs* in that *tbabs* does not specify the type of absorption occurring. If necessary, we are able to modify each of the absorption models in detail, picking the abundance of the elements in the ISM. However, for the time being we set the model to its default parameters, as we assume the ISM does not vary greatly from what is considered to be normal ISM abundances. In the case of DEM L71, we most likely need to apply two different absorption models: one to account for the LMC and another for the Milky Way. The elemental abundances and dispersion throughout each of the galaxies is different, and thus it affects the incoming X-rays in different ways. Additionally, the X-rays from the LMC are more absorbed than they would be only passing through the ISM of a single galaxy, which is difficult to capture in a single absorption model.

The emission model we have chosen to use is *vnei*, a non-equilibrium ionization collisional plasma model that allows us to control the abundances of the elements. As discussed earlier, non-equilibrium ionization means the plasma temperature and the number of ions are not directly correlated because of the time-dependence of the ionization process of the atoms and ions. We are assuming that the plasma is in this state due to the low density of a SNR [1]. With this model, manipulation of the abundances in the SNR is more important than in the absorption models, as the abundances can change drastically throughout the SNR.

In addition to the models, we are using a set abundance for all of the elements in the models. There are two pre-determined abundance settings in particular that relate to the abundances in the LMC: 1) Wilms and [4] 2) Anders and Grevesse [5]. We also set all of the abundances of the main elements (He, C, N, O, Ne, Mg, Si, S, Ar, Ca, Fe, and Ni) to 0.3, the abundance of the elements in the LMC relative to solar (our sun).

Chapter 4

Research Methods

In order to further study the area of interest found in DEM L71, we must study the specific properties of the area of interest and surrounding regions. We extract spectra from designated areas shown in Figure 4.1. The area of interest was approximated and fit with a rectangle. All of the surrounding regions mirror the same shape, dimensions, and angle orientation as the rectangular region of interest, but positioned across the SNR in order to obtain a comprehensive view and uncover any possible trends in the spectra. In addition, spectra were extracted from the adjacent, left and right, regions to the area of interest. Source free background regions were selected from very large regions of the sky near the area of interest. A larger background region leads to a more accurate representation of the background and its successful removal via subtraction during spectral analysis.

The regions of spectral extraction are first designated in ds9, a software for astronomical imaging and data visualization, by overlaying the rectangles onto the median energy image. The regions were saved in a format that is compatible with CIAO and Sherpa. The spectra were then extracted from the regions using the *specextract* command from CIAO, in which the source background spectrum was also identified, so it could later be subtracted from the source spectra. Extracted spectral files were created in this process, which could later be imported and analyzed in Sherpa. Fi-

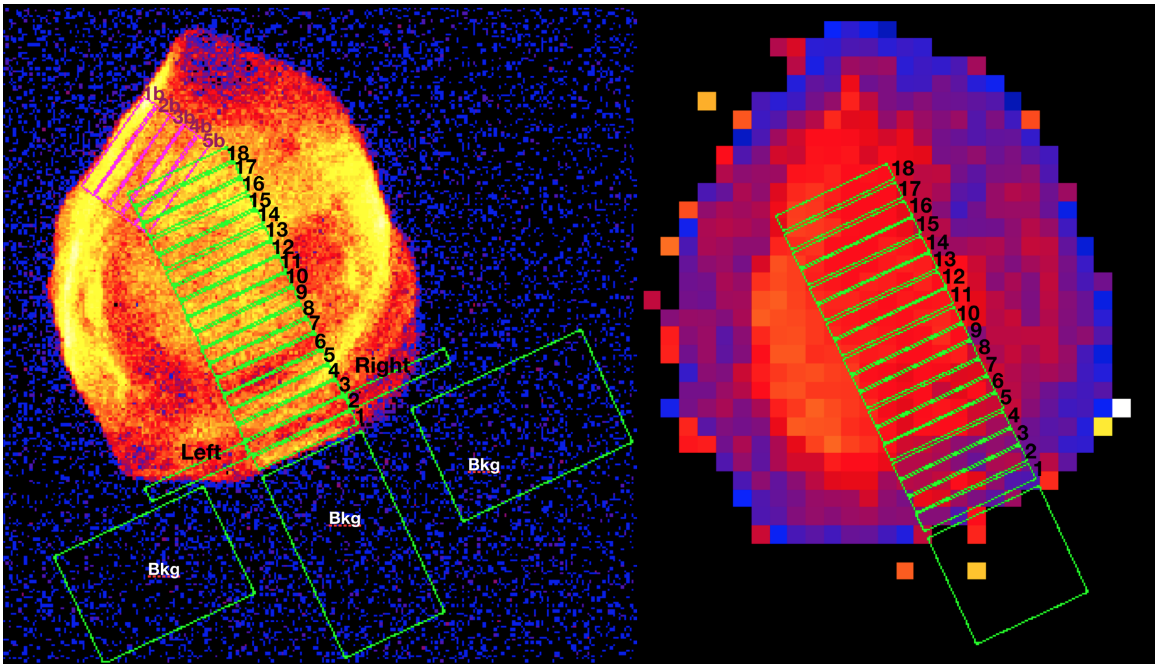

Figure 4.1: Indicated and numbered regions from which spectra of DEM L71 were extracted. Background spectra are also indicated as it was subtracted from the spectra in DEM L71. The spectra regions, initially made on the median energy image (right), are overlaid on the counts image of DEM L71 (left) to show how the area of interest (region 2) lies in a low counts area.

nally, we binned data points in the initial spectra. Doing so significantly increases the signal-to-noise ratio of the spectra making trends and comparisons much easier. This was done using the Sherpa command *group_counts(15)*. We chose to combine 15 counts as it reduced the amount of noise, without losing details in the spectra.

An example of the spectra extracted and binned can be seen in Figure 4.2.

After grouping photon counts, we apply the photoelectric absorption and non-flux ionized plasma models (*phabs* and *vnei* respectively). Each of the models comes with a set of parameters, N_H, kT and τ that can manually be changed or left as free parameters for Sherpa to find a value that produces the best spectral fit. Reference elemental abundances are set to a predetermined abundance (Wilms or Anders and Grevesse). A good fit will produce a chi-squared value close to one, calculated by

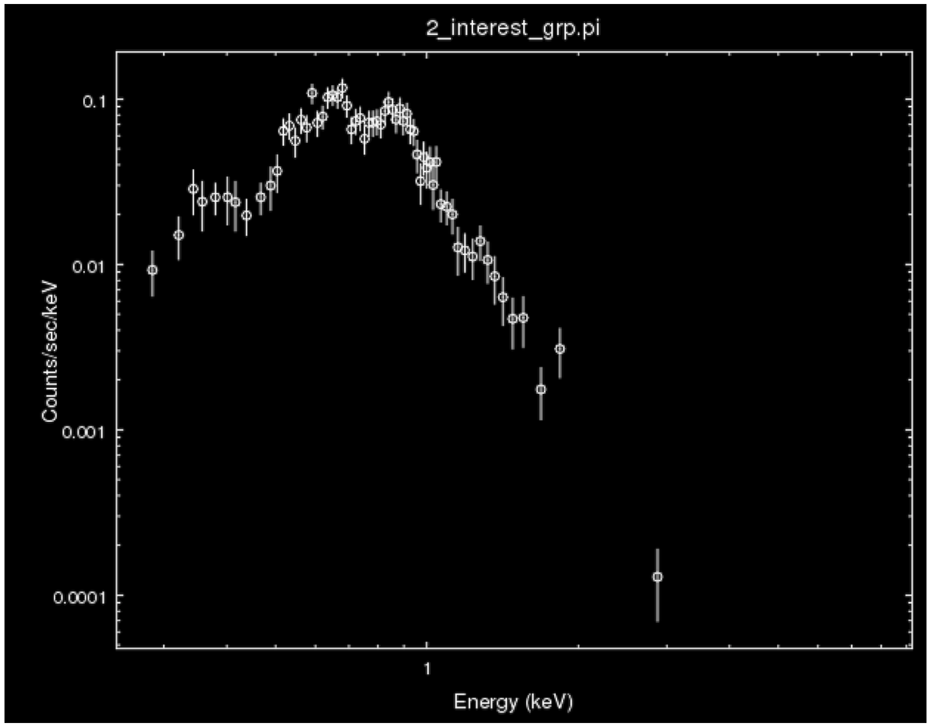

Figure 4.2: Soft X-ray spectra for the area of interest. This data comes from observation id 775 which consisted of a 42.62 ks exposure time. All data points shown represent a group of 15 X-ray photon counts, done using the command group_counts(15).

Sherpa, while bad fits will result in a chi-squared that deviates significantly from one. We alter the relative elemental abundances and N_H, kT and τ values to obtain the best fit (chi-squared close to one) to the data.

4.1 Multiple Component Models

Due to the 3-dimensional nature of the SNR, often times some regions may contain both ejecta and shocked ISM emission. To account for this we may use more complicated models such as the addition of two plasma temperate models using the command *set_source(id, xstbabs.abs*(xsvnei.snr+xsvnei.ism))*. From this we can control the relative abundances and timescale parameter values for each model independently. An example of this code is shown in Appendix A.3.

4.2 Spectra Extracted

There were many regions of DEM L71 covered by extracted spectra. A full understanding of the remnant on a global scale is key to understanding the general behavior of the SNR to identify the underlying physical processes in the high energy, but low counts density, area in the south east edge of DEM L71.

4.2.1 Diagonal Spectra

The diagonal spectra can be seen in Figure 4.1. These spectra allow a full study of the evolution of the abundances and timescale parameters across DEM L71 with a direction governed by the area of interest orientation. Through analysis of the spectra, we were able to identify a nearly identical spectra to region of interest. Region 6 borders the higher count ejecta and it resides in the higher median energy ejecta region as seen in Figure 4.1. Figure 4.3 shows a comparison of the region 2 and region 6 spectra, which are very similar.

4.2.2 Transverse Spectra

We had previously studied the evolution of DEM L71 through the orientation of the area of interest. To further understand the global properties of the SNR we need to study more of the remnant. This set of spectra, shown in Figure 4.4, are designed to better probe the shocked ISM to ejecta. Several rectangular regions encapsulate dense ISM regions of the SNR and center rectangular sections encompass the ejecta. Highlighting these regions allow with the transverse spectra allow us to compare spectrum extracted from similar regions defined in the diagonal spectra, i.e. the ISM and ejecta.

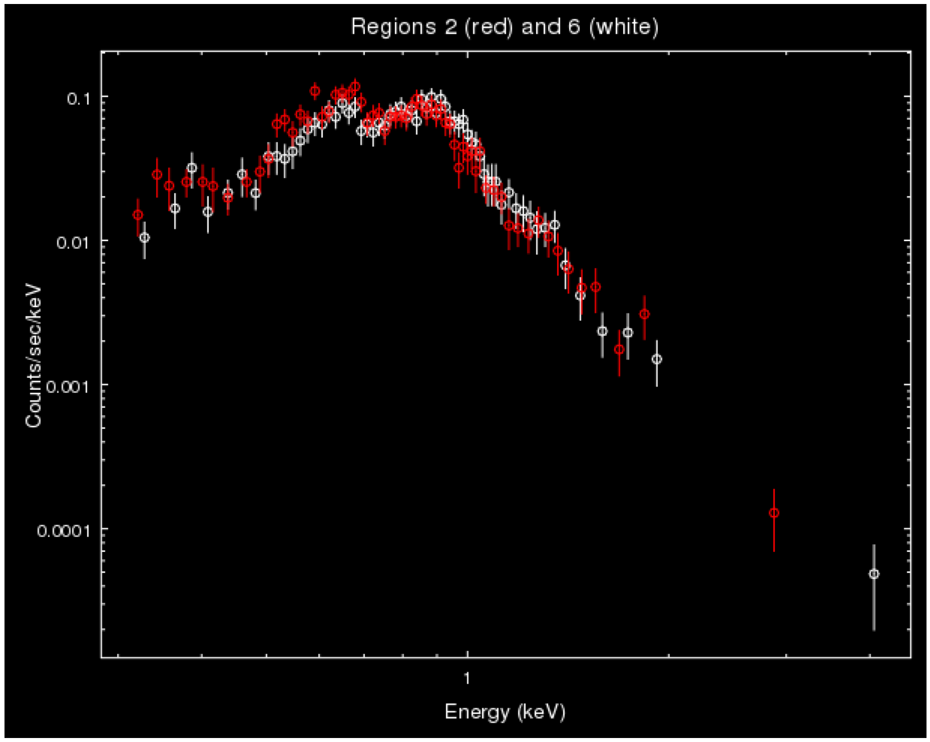

Figure 4.3: The red data points show the spectral data of the area of interest, region 2, and the white data points show the spectral data extraction from diagonal region 6.

4.2.3 Spectral Analysis of Extraction Regions

In order to understand the cause of a small scale structure, we first need to understand the behavior of the timescale parameters and elemental abundances on a global level. We used the regions identified by the diagonal spectral extraction regions, Figure 4.1, and the transverse regions, Figure 4.4. Each of the regions were studied individually to create the best possible fit to the spectral data. After obtaining all of the fit values we plotted them sequentially to watch their evolution across DEM L71.

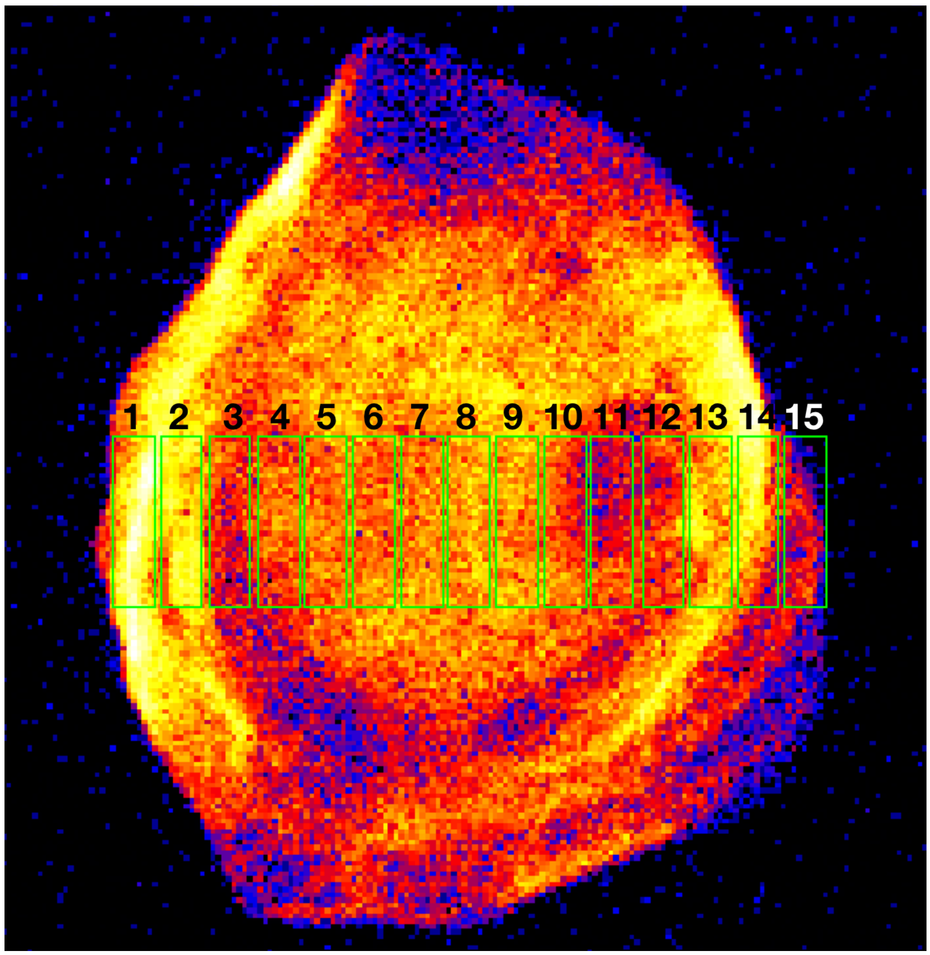

Figure 4.4: Regions indicated show where spectra was extracted west to east across DEM L71.

Chapter 5

Results

5.1 Diagonal Spectra

All spectral extraction regions are show in Figure 4.1. Figure 5.1 shows the resulting timescale parameter values from spectral fits and their evolution from region 1 to 18.

In general, there does not seem to be a global trend with the N_H and kT values. The few places where a trend may be argued are the last four point of the N_H plot and the first three points of the kT plot. Deciding whether or not these trends are existent is tricky as the value of a single parameter also depends on the values of all of the other values. There may be over compensation by one of the timescale parameter values, say τ, if the N_H or kT value is too low. In these cases we say that the fit has found a minimum. This may be the case for the last three points on the N_H plot, spectra numbers 16, 17 and 18. While the values of the column density decrease, the values of the ionization timescale increase which could be an indication of overcompensation. An additional indication that this may not be an accurate value is the value of τ should be the roughly the same places of equal distances from the center of the SNR. Ionization timescale is the time since the material has been shocked. We assume that time to be approximately the same at those places with

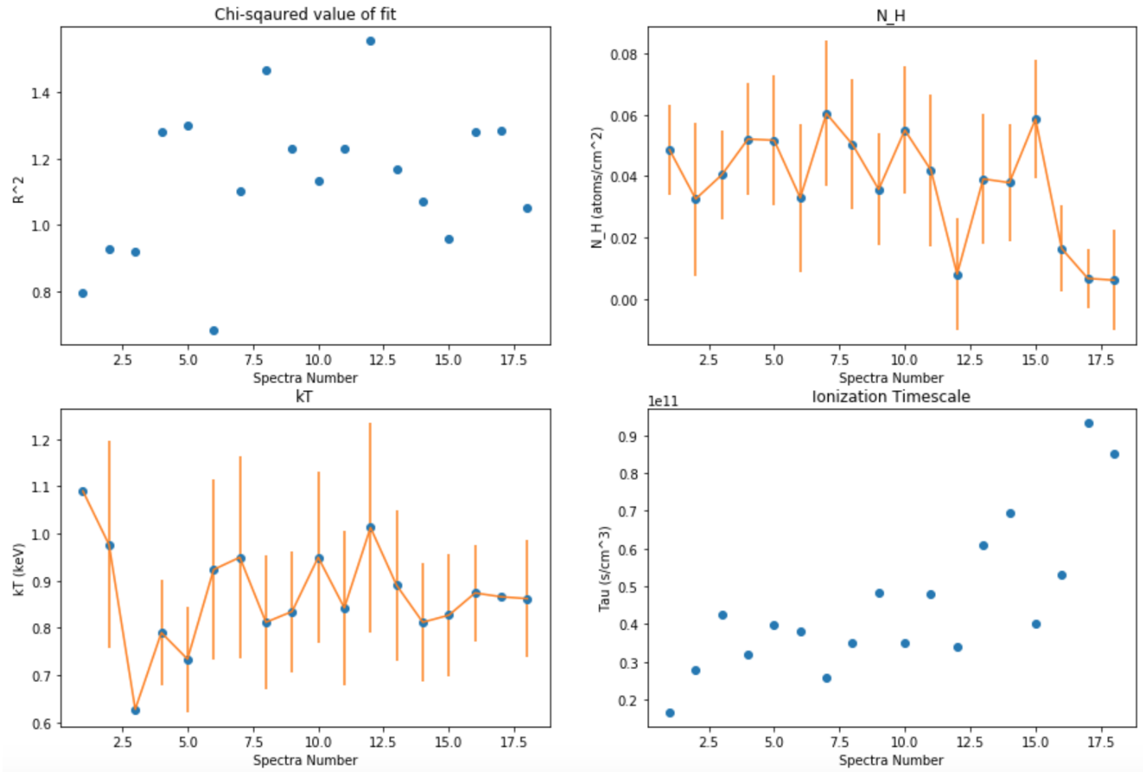

Figure 5.1: Timescale parameter values, kT, τ, and N_H, of all 18 spectra outlined in Figure 4.1. All values are the result of spectral fits applied to the individ ual spectra.

equal distances from the center. Spectra 17 and 18 have the highest τ value and do not have an approximate pairing on the other side of the center of the SNR.

Overall, it appears there is a trend in the ionization timescale plot, but this is not conclusive. When fitting the spectra, the τ values did not come with any errors. More significant errors can be calculated using the computationally demanding sherpa command *conf()* as future work. This command calculates the expected value for the parameters and the 68% confidence interval. Understanding these values with the errors will tell us if there is actually a trend in the data, or if all points are within error and do not indicate a trend.

We also plotted the evolution of the abundances of O, Ne and Fe across DEM L71 shown in Figure 5.2. As we move into the SNR, the amount of O decreases then

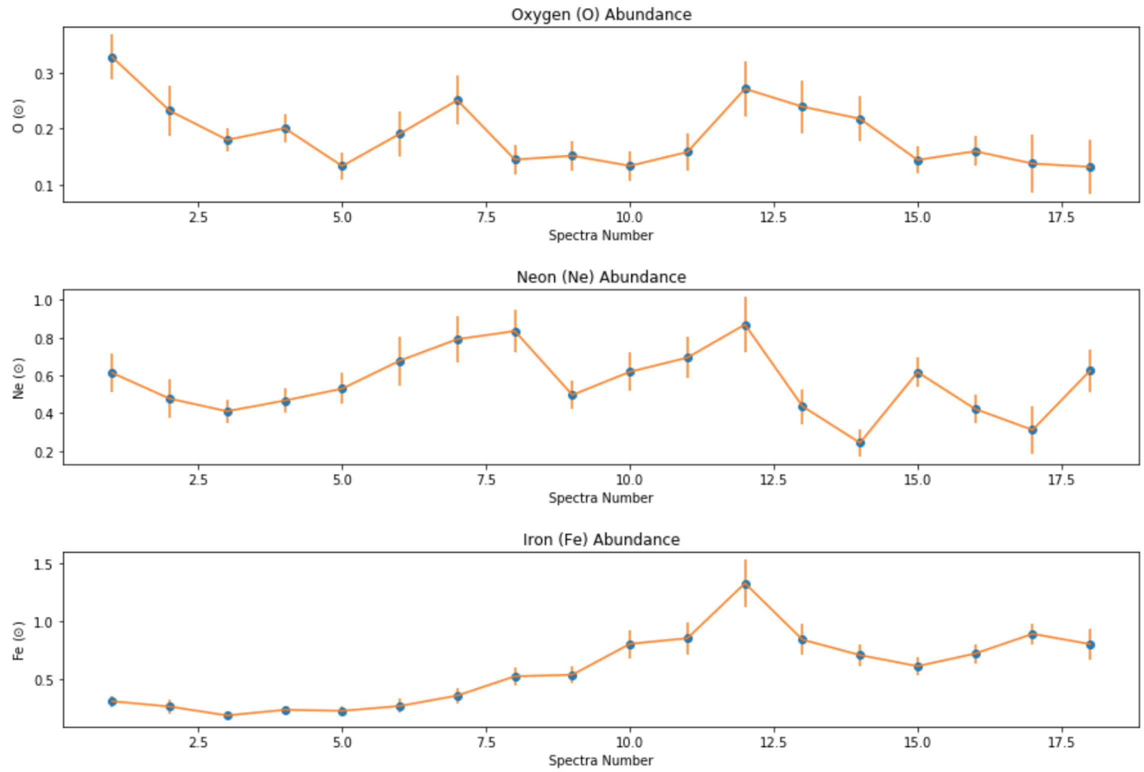

Figure 5.2: The abundance values of the three thawed elements, O, Ne and Fe for all 18 spectra fits of the identified diagonal spectra in Figure 4.1.

comes to a peak in spectra on either side of the middle of the ejecta. In the middle of the ejecta the amount of O is at a minimum. Ne follows a lesser but similar trend. Fe does the opposite, increasing in abundance as the spectral extraction regions get closer to the center of the SNR and peaks at region 12, the same region where O and Ne also reach a peak. We expect to see this sort of trend in the abundances because during the supernova explosion, there is mixing of ejecta and the material is so hot it becomes a plasma. As the plasma cools down and recombination occurs we begin to see the existence and location of elements through the emission lines. Iron is a heavy element and is the last element formed in a star so in general it should be located more in the central part of the explosion.

5.2 Transverse Spectra

Figure 4.4 shows the identified spectral regions used to determine the timescale parameter values recorded in Figure 5.3. The x-axis organization for the transverse spectra has been altered from that used for the diagonal spectra. In the diagonal spectra plots, we simply identified the number of spectral extraction region. We used a relative distance value from the middle region, region 8, for the transverse spectra. This is the 0 point on the x-axis. Region 8 was identified as the middle of DEM L71 meaning that we expect to see the most relative ejecta in this region because the outside shell of ISM is at its thinnest. This distinction become more important later on as we try to identify the regions in which the ejecta dominates the spectra and where the ISM dominates the spectra (further discussed in 5.3).

Behavior of the timescale parameters calculated from the transverse spectral regions are shown in Figure 5.3. Column density, N_H has a varying value with an overall decrease in column density in the middle of the DEM L71. In this case the middle of DEM L71 is 0 on the x-axis, the middle of region 8. This result coincides with the higher median energy of the ejecta. A lower N_H means there is less absorbing material between the observer and the object resulting in the detection of more low energy X-rays by the observer. Therefore, the median energy of the ejecta must be the actual median energy of the material and not a result of a secondary characteristic such as a high N_H value. Similarly, the kT values, plasma temperature, of the transverse spectra almost all result in the same value. Region 3 has an anomalously high kT value. Additionally, the N_H value of region three is lower that surrounding N_H values. Both values have a large uncertainty values and are a local minima and global maxima, of the N_H and kT plots respectively, indicating that these values may be the result of the spectral fit finding a minima. It is possible that these values are

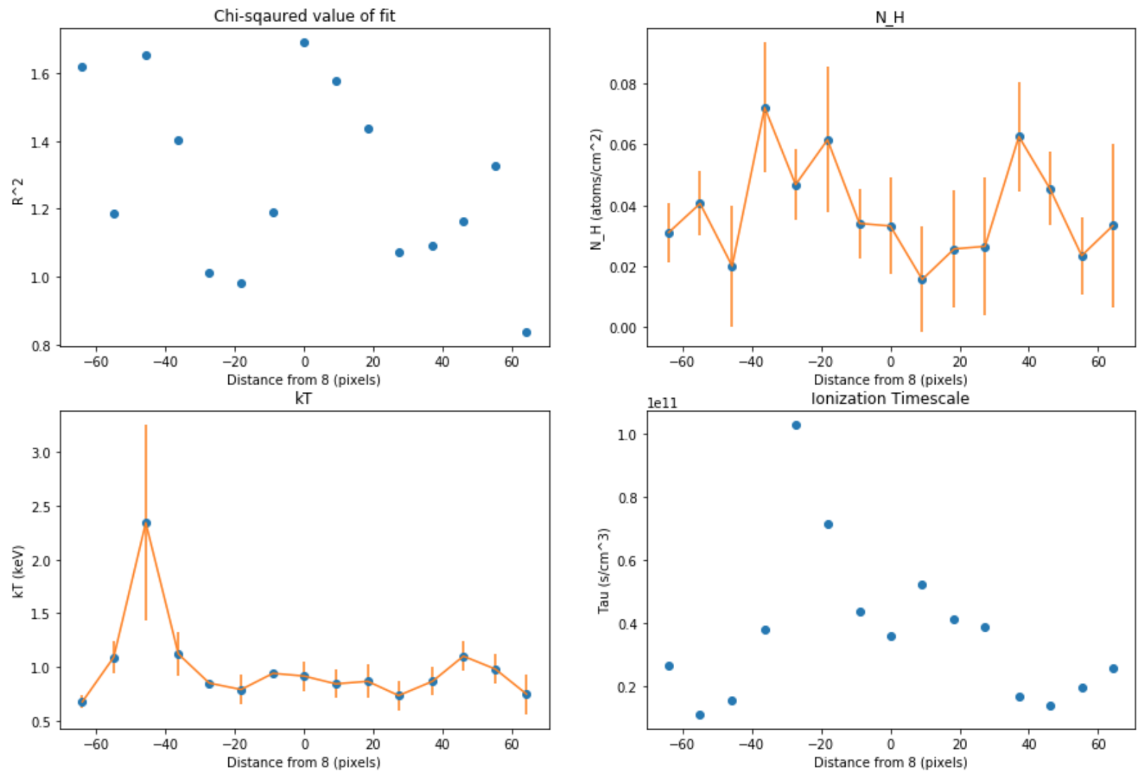

Figure 5.3: The abundance values of the three thawed elements, O, Ne and Fe for all 18 spectra fits of the identified transverse spectra in Figure 5.3.

representative of the characteristics of region 3, but most likely not to that extreme.

Just as with the extreme region in the kT fits the τ value for region 5 reaches a global maximum. Again, there were no error bounds generated for the timescale parameter values so we are unsure of the uncertainty on these points. This high value may be the result of a minima in the spectral fits or it could be representative of the actual value. In a SNR there is the contact discontinuity which marks the distinction between the material shocked by the forward moving shockwave and material chocked by the reverse (inwards moving) shock wave. Material located at the contact discontinuity would have the longest τ value as the reverse shock would have been generated by the forward shock at this point and all other material both in front of and behind of the contact discontinuity would be shocked more recently or still has

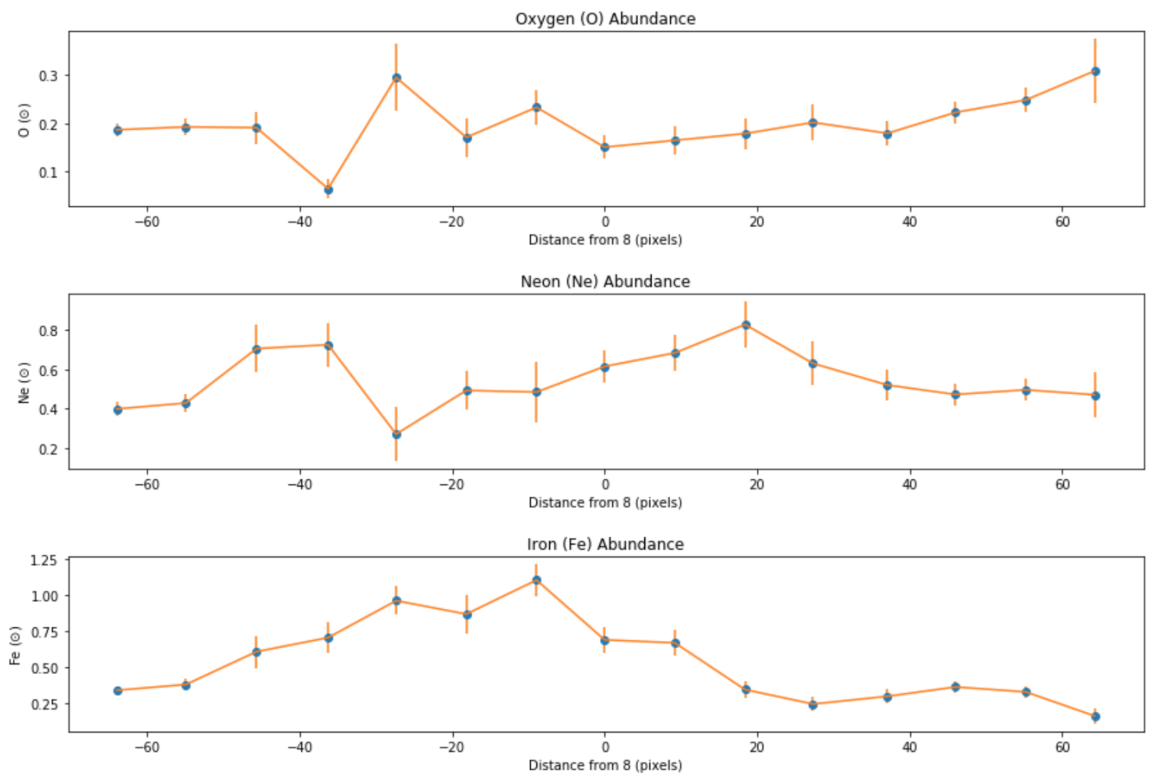

Figure 5.4: Timescale parameter values, kT, τ, and N_H, of all 15 transverse spectra outlined in Figure 4.4. All values are the result of spectral fits applied to the individual spectra.

yet to be shocked. The existence of the contact discontinuity may be an explanation for the high τ value at region 5, where the contact discontinuity is the brightest. As with the entire SNR, the contact discontinuity is a 3-dimensional feature so we should see areas on the right side of DEM L71 that share a similar high τ value as region 5. Studying the rest of the τ data points, there are no further peaks in the ionization timescale values.

We also wanted to study the abundance of what we identified to be three of the most important elements in the fit of the spectrum: O, Ne and Fe. The results of the abundance values are shown in Figure 5.4. Abundances of Fe and Ne corroborate what was seen in the diagonal spectra: an increase in Fe into the middle of the SNR and peaking near the center, and the opposite behavior of Ne. O, however, does not show a large dip in abundance in the center as was seen in the diagonal spectra. What is significant is that the abundance values match where there is overlap. We model a selective abundance of O of about 0.15 in the center of DEM L71 in both the transverse and diagonal spectra.

5.3 Ejecta and ISM Models

From the median energy of DEM L71, Figure 2.3, we can see that the median energy of the region of interest, 750 eV, closely resembles the median energy of the ejecta material. This suggests that the possible cause for the region of interest, is that ejecta material dominates in the region of interest. Having an excess of ejecta material relative to the regions surrounding the region of interest would result in an increase of the median energy of the region of interest, which is what we see. This hypothesis is supported by analysis of timescale parameter values measured from clearly ejecta dominated regions of DEM L71 as formed by several different research groups summarized in Frank et. al. [6].

We wanted to test the hypothesis that an excess of ejecta material in region 2 is causing the high median energy. To do this we developed two spectral models, one of the ejecta material (further in subsection 5.3.1), and the other of the interstellar medium (ISM) (subsection 5.3.2). We extract and fit spectra from regions of DEM L71 that best represent the ejecta and ISM and then combine the abundances and timescale parameters for each of the two general fits to create the most representative models of the ISM and ejecta. Each of these models is then applied to the single extracted spectra of region 2 (following the procedures outlines in 4.1). The resulting fit tells us the relative weight of each of the two models. In order for our hypothesis to hold true, the ejecta model should have a higher influence on the fit for region 2 than the ISM model. The relative weights are determined from the normalizations. However, another possibility is the ISM model may have more of an influence than the ejecta model, but the ejecta model is more prevalent in region 2 than any of the surrounding regions. If the fits of the regions surrounding region 2 have a lower normalization value for the ejecta model then we can argue that the median energy is visible not because it is unique itself, but because of the area it lies in. An average median energy (750 eV) residing in a region that is all low median energy values will stick out. Fitting region 2 alone is not enough, both of the derived models must also be applied to all surrounding regions of the the area of interest. These regions include regions 1, 3, left and right as seen in the Figure 4.1.

Figure 5.5 shows the resulting fits of both the ejecta and ISM models. These models were applied to spectra from the anomalous energy feature.

5.3.1 Ejecta

The ejecta in DEM L71 lies in the center of the remnant. It is the stellar material that was expelled into space by the supernova explosion in comparison to the ISM which gets picked up by the expanding shock wave. Figure 5.6 shows the regions used to extract spectra and create the ejecta model from. The center of the remnant is the best place to collect values due to the geometry of a sphere projected onto a flat plane. Along the rims of the remnant we see the densest collection of the ISM collected onto the outer rim. As you move to the middle of the approximately circular remnant the amount of ISM we are looking through becomes thinner, until it reaches a minimum in the very middle. Also at this point in the center of the SNR, the thickness (optical depth) of the ejecta is at a maximum. Because of this it is best to determine the ejecta model using spectra extracted from the middle of the remnant where we can assume the influence of the ISM is at a minimum.

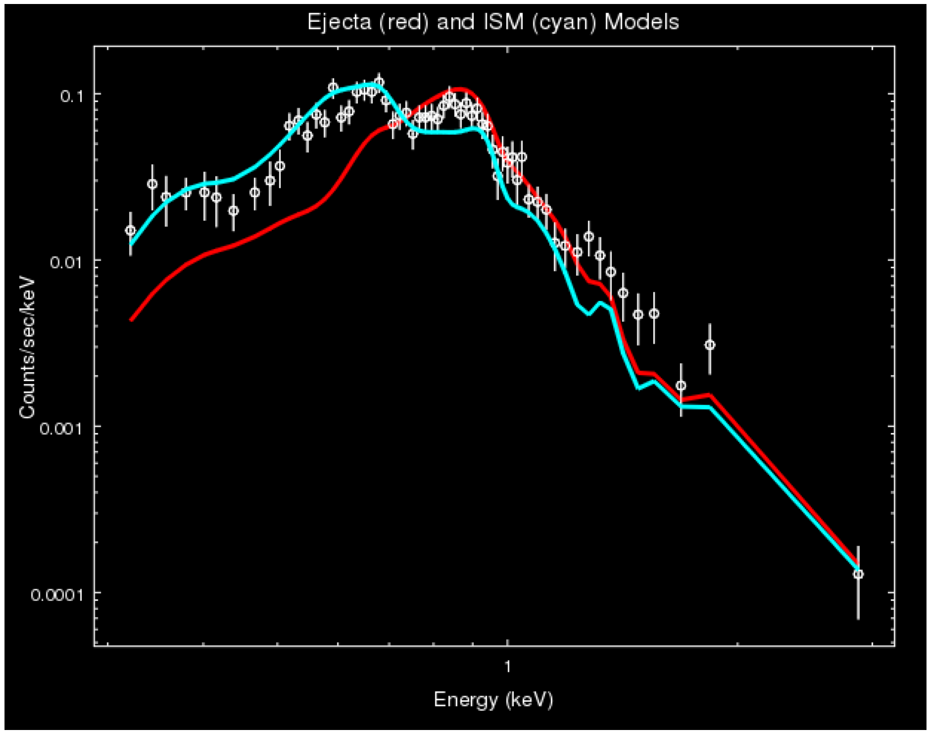

Figure 5.5: Ejecta (red) and ISM (cyan) models fit to spectral data from the region of interest, region 2.

The transverse and the diagonal spectra overlap in the middle of the supernova remnant as shown in Figure 5.6. Models for each of the spectra regions identified were created and averaged together for and ideal ejecta model. An improvement to this model could weight each of the values with respect to how far away they are from a perfect fit, how far the chi-squared value of the fit varies from one. Resulting values from all fits of the ejecta spectra can be found in Table 5.1.

5.3.2 ISM

As the outward moving shockwave expands into the interstellar medium, ISM, it sweeps up material which becomes heated and shocked. The ISM is not material created by the supernova explosion itself, but rather material that was already in space. An active progenitor star may have thrown out material into space or previous

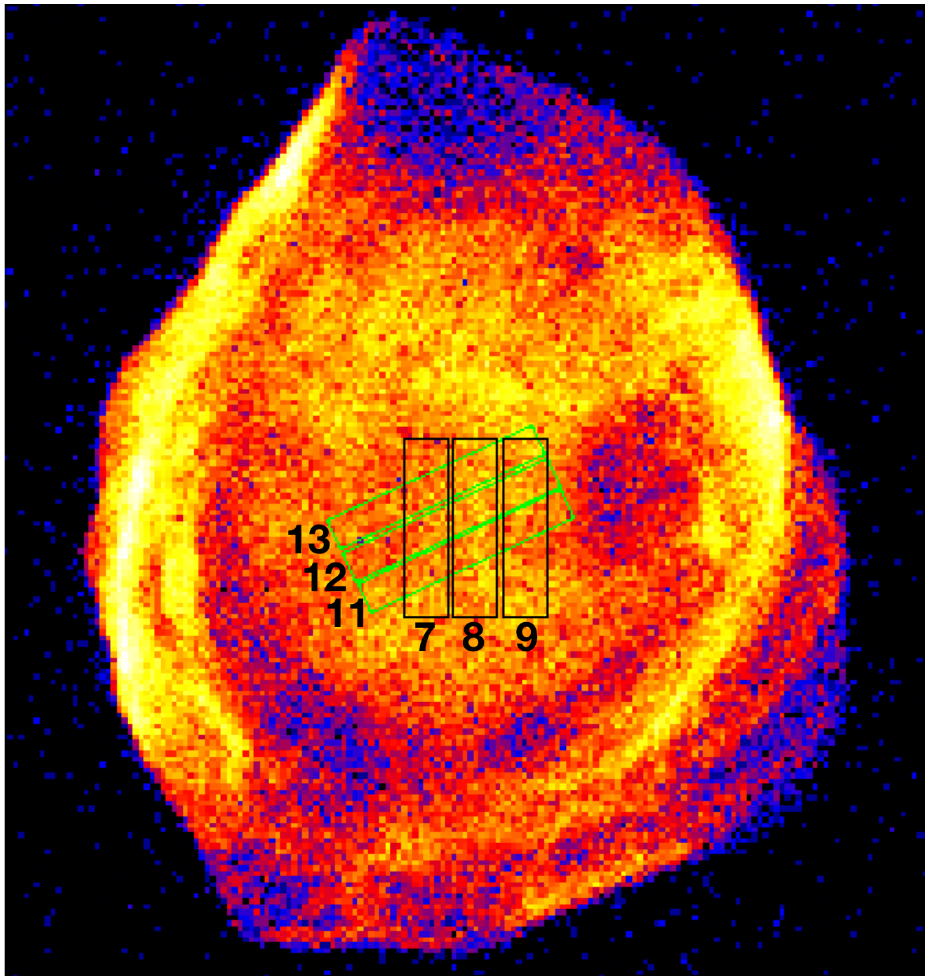

Figure 5.6: Regions indicated were used to create the ejecta model. The green regions (11, 12, 13) come from the diagonal spectra while the black regions are from the transverse spectra (7, 8, 9).

Spectra	r^2	$N_H(\frac{atoms}{cm^2})$	kT (keV)	$\tau(\frac{s}{cm^3})$	O ($\odot$)	Ne ($\odot$)	Fe ($\odot$)
11	1.25	0.03±.02	1.0±0.2	3.40e+10	0.18 ±0.04	0.6±0.1	1.0± 0.2
12	1.52	0.02±0.02	0.9±0.2	4.72e+10	0.19±.04	0.37±.09	0.8± 0.1
13	1.17	0.03±0.03	0.8± 0.2	6.09e+10	0.23±0.05	0.43±0.09	0.8±0.1
7t	1.16	0.038	1.0±0.1	3.64e+10	0.23±0.03	0.4±0.1	1.1±0.1
8t	1.69	0.02±0.02	0.9±0.2	3.53e+10	0.17±0.03	0.50±0.08	0.7±0.1
9t	1.57	0.02±0.02	0.8±0.1	4.8e+10	0.14±0.03	0.7±0.1	0.64±0.09
Average		0.03	0.9	4.36e10	0.19	0.5	0.8

Table 5.1: Values of spectral fits for ejecta model.

supernova would have created material that then sat in space until collected by the shock wave. Stellar winds from the progenitor star could shape the ISM material making it denser in some areas and further mixing the material.

The best location on the SNR to extract spectra from and model the ISM is on the outer rim as it has collected on the forward moving shock wave. Figure 5.7 shows the region drawn from which data was extracted to model the ISM. Although it should be the same all around the perimeter of the SNR, we decided the best location to model the ISM was immediately next to the region of interest as this would be the ISM influencing the spectra of the region of interest if it is ISM dominated. Additionally, we drew a large polygon area to extract data from because the outer rim has a lower photon density that the ejecta region. Making a single large region is the same as making many smaller regions and adding all of the values together like was done for the ejecta model. Resulting values of the ISM fit can be found in Table 5.2.

We use the N_H value from the ISM model instead of the ejecta model. Column density is not a result of the conditions in a SNR, it is the conditions of space between the observer and the object being studied. Due to this we want an N_H value from as near to the area of interest as possible which leaved the ISM model. The ISM model was taken from an area of DEM L71 geographically close to the area of interest, just south - south-east of the region. Doing so we make an assumption that the column density does not change significantly over "short" distances.

Spectra	r^2	$N_H(\frac{atoms}{cm^2})$	kT (keV)	$\tau(\frac{s}{cm^3})$	O ($\odot$)	Ne ($\odot$)	Fe ($\odot$)
Polygon	1.01	0.03±0.02	1.0±0.2	1.47e+10	0.37±0.04	0.67±0.08	0.28±0.04

Table 5.2: Values of polygon spectral fit for ISM model.

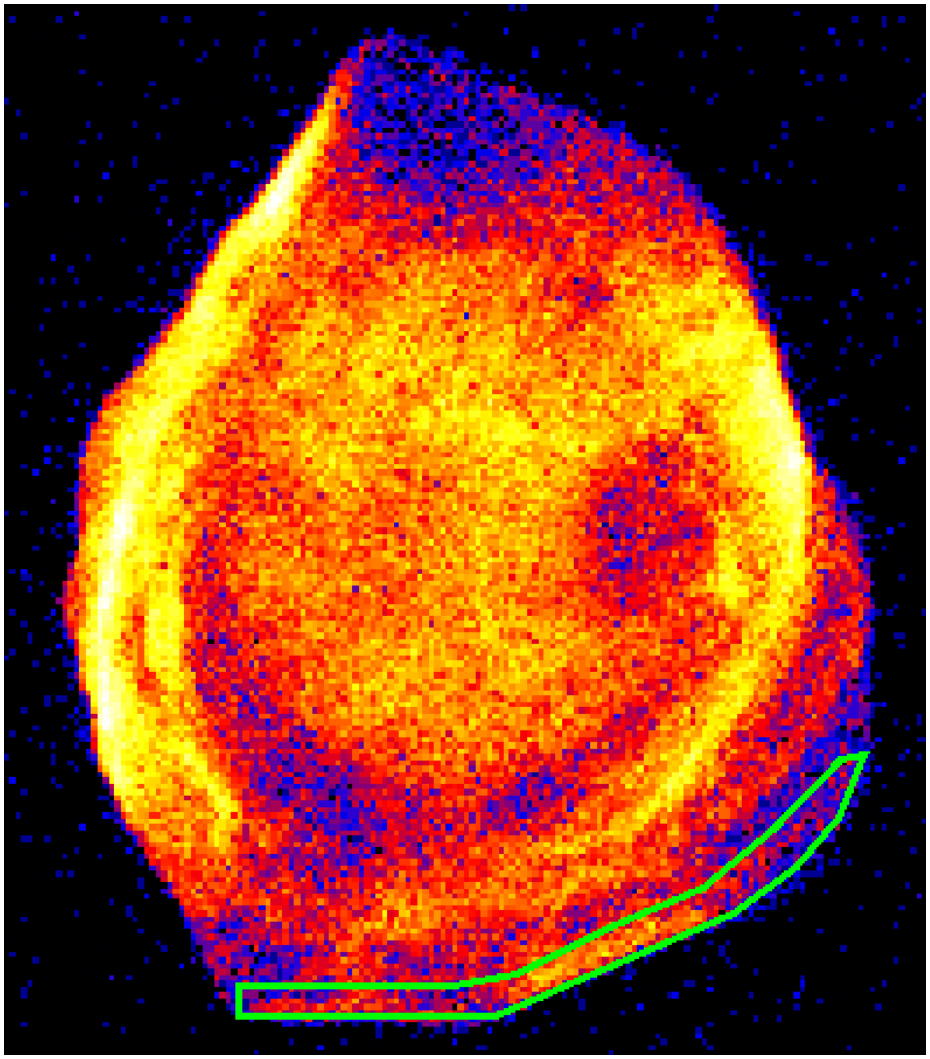

Figure 5.7:

5.4 Results of Model Fitting

We applied the ejecta and ISM models to the region of interest keeping all pre-determined element abundances and timescale parameter values set to the representative values for ISM and ejecta. The only value we allowed to vary is the normalization. This value tells us the approximate weight of each of the models. Both of the models were applied to the region of interest as well as the surrounding regions. Doing so covers the possibility that there may be more ejecta in the region of interest than surrounding regions, making it appear as an excess of ejecta. Resulting normalization values from model fits are shown in Table 5.3.

Spectra	r^2	Ejecta	ISM	Energy Flux $\frac{Ejecta}{ISM}$
1	0.71	1.2e-05±2.6e-06	5.0e-05±2.1e-06	.15
2	0.94	1.7e-05±2.2e-06	2.6e-05±1.7e-06	.32
3	0.84	1.2e-05±2.6e-06	5.1e-05±2.1e-06	.15

Table 5.3: Normalization values for ejecta and ISM model fits to region of interest and surrounding regions.

The final column of the table shows the normalized ratio of the energy flux for each of the spectra. This value has been calculated to create an easy interpretation of the relative weights of the ejecta and ISM models for each of the spectra indicated. To calculate this value we ran the command *calc_energy_flux{lo=0.3,hi=7.0,id= }* which calculates the integral of the energy multiplied by the spectral model for each designated area. The highest ratio values comes from spectra 2 which is the region of interest. Even though spectra 2 is not completely dominated by the ejecta model it produces an energy flux ratio 2.1 times greater than the next highest, .1555 from spectra 1. A higher contribution of ejecta emission in region 2 than in surrounding regions is more apparent than if region 2 were closer to the ejecta (region 6 and higher). With the ejecta material comes the higher median energy explaining the resulting energy feature in a low counts area. Region 2 produces a higher proportion of higher median energy values than surrounding regions.

5.4.1 Physical Interpretation

What now needs to be explained is how extra ejecta material made its way into region 2. There are two main possibilities as to the existence of the ejecta in region 2. Either the ejecta has always been in the region, or it travelled from the ejecta in the center of DEM L71 to the southeast rim. This could be done by a velocity kick. However, if the extra ejecta was preexistent we would not know the depth location of the material and if it truly located on the outside rim, region 2, or if just appears to be.

In order for the ejecta to have travelled from the center of DEM L71 to the southeast rim, some ejecta needed an additional velocity component. The velocity component may be a result of the initial supernova explosion which was very turbulent and created an asymmetrical distribution of velocity in the surrounding material. An interesting question brought up with this explanation is why there aren't any other energy anomalies such as this one in other area of DEM L71.

Additionally, if an extra velocity component is the reason for the existence of this feature it makes physical sense for regions 1 and 3 to have trace amounts of ejecta playing into their spectra. If the region was created from a lump of ejecta that has travelled outwards and populated the region of interest there will be natural variations in the velocity of the dust particles and ions in the general lump. Some may be moving a little faster and have made their way into region 1 and some with lesser velocity stayed in region 3. A majority of the particles will fall into an average velocity range which populates region 2, the region of interest.

Another possible explanation for the existence of this feature is a geometric trick. When looking at the image of DEM L71, we a see two dimensional projection of a three dimensional object so we loose all depth perception of material in the SNR. The material that we are seeing in region 2 may be closer to the center of DEM L71 but we are seeing it as next to the outside edge of the remnant due to a projection effect.

Chapter 6

Conclusion

In this research we were able to identify a new energetic feature in SNR DEM L71 and characterize the parameters and origin of the energetic feature. Using spectra extracted from the center of DEM L71, where we can assume there is little to no contribution from the ISM in the extracted spectra, we were able to create a spectral model for the ejecta. Outside edge regions on the south east rim were identified for use in creation of the ISM model as the edge of a sphere is the densest region for the outside edge. Therefore it is the densest collection of ISM. After creating the models, we applied them to the region of interest and surrounding regions. We only varied the normalization to determine the weight of each of the two models applied. Region 2, the region of interest, had the highest ratio of ejecta model normalization to ISM model normalization with a ratio of 0.32. We can interpret this ratio as the approximate values of each material in the individual regions each spectra was extracted from. From the ratio value of 0.32 we see the ejecta is not completely dominating, but there is a higher collection of ejecta in the region of interest than in surrounding areas: 1, 3, as seen in Figure 4.1. The next highest ratio of ejecta to ISM are in regions 1 and 3. Data analysis is not presented for other regions.

An addition of ejecta material to region 2 more so than surrounding regions explains the higher median energy value, the energy anomaly first discovered in the median energy image of DEM L71, Figure 2.3. Ejecta in DEM L71 has a higher median energy of about 750 eV and higher. Figure 2.3 shows similar contour levels of energy 750 eV at the ejecta and the region of interest. It makes sense that the contour level would match if the material in the region of interest is composed of ejecta as well as ISM. The higher median energy of the ejecta will skew the median energy of that region to a higher value than surrounding regions due to the higher proportion of ejecta in region 2 than surrounding regions.

A possible physical explanation for the existence of extra ejecta material in region 2 is some ejecta material were given an extra velocity component during the supernova explosion and propelled to the outer south-east rim where we now see it. Supernova explosions are more often asymmetrical than symmetric so an extra bit of velocity of ejecta in one direction is not completely unlikely. The region of interest could also be the result of a projection effect. We do not have depth perception into the material we are studying and as such as are unaware if the high energy material is closer to us, further away, or in the middle of the SNR in that region.

Although we cannot conclusively say why the high energy feature is there, we believe we have identified the cause of the structure, a higher abundance of ejecta material than surrounding regions.

6.1 Future Work

Further analysis work on the region of interest, surrounding regions, and on a global SNR scale have been alluded too, but will be summarized. The analysis done so far has used a single observation of DEM L71. In the Chandra archives are three separate observations that could all be used and stacked on top of each other. This would increase the number of counts available for all of the models and decrease the uncertainties on all of the measured timescale parameter and abundance values.

Additionally, in the spatial distribution plots of τ, Figures 5.1 and 5.3, there are no error bars. We do not know what any of the uncertainty values are for any of the τ values and thus cannot confidently identify a trend in the data.

Finally, we could apply the median energy technique to other SNR. We do not know how many undiscovered energy features are in existence. It is unlikely that we happened to pick one of the only SNRs with an energy anomaly to first apply the statistical technique too. More likely, there are many undiscovered energy structures in SNRs and other structures. Applying this technique to more structures and determining the cause for the energy features may indicate that there is something missing in our understanding in the formation and evolution of SNR. For this reason alone, this technique should be applied more broadly.

Appendix A

CIAO and Sherpa Spectral Analysis

A.1 Spectral Extraction

The following shows the commands used in CIAO to extract spectra from designated spectral extraction regions, Figures 4.1 and 4.4. File names used are representative of the region of interest.

```
punlearn specextract

pset specextract infile="acisf00775_repro_evt2.fits[sky=region(2_interest.reg)]"

pset specextract outroot=2_interest

pset specextract bkgfile="acisf00775_repro_evt2.fits[sky=region(background.reg)]"

specextract mode=h
```

A.2 Spectral Fitting

These commands are used to load the extracted spectra into Sherpa, apply an absorption and emission model to the spectra and fit the spectra. File names used are representative of the region of interest.

```
load_data(2,'2_interest_grp.pi')

ignore(':0.3,7.0:')

subtract(2)

set_xlog()
```

```
set_ylog()

set_source(2,xstbabs.abs2*xsvnei.snr2)

for i in snr2.param[2:14]:
i.val=0.3

thaw(snr2.O)

thaw(snr2.Ne)

thaw(snr2.Fe)

fit(2)
```

A.3 Multiple Component Models

These commands are used to load the extracted spectra into Sherpa, apply a single absorption model and two emission models to the spectra (ISM and ejecta models) and fit the spectra. File names used are representative of the region of interest.

```
load_data(2,'2_interest_grp.pi')

ignore(':0.3,7.0:')

subtract(2)

set_xlog()

set_ylog()

set_source(2,xstbabs.abs2*(xsvnei.snr2+xsvnei.ism2))

for i in snr2.param[2:14]:
i.val=0.3

for i in ism2.param[2:14]:
i.val=0.3

snr2.kT=0.9

freeze(snr2.kT)

snr2.Tau=4.36e+10

freeze(snr2.Tau)

snr2.O=0.19
```

```
snr2.Ne=0.5

snr2.Fe=0.8

abs2.nH=0.03

freeze(abs2.nH)

ism2.kT=1

freeze(ism2.kT)

ism2.Tau=1.47e+10

freeze(ism2.Tau)

ism2.O=0.37

ism2.Ne=0.67

ism2.Fe=0.28

fit(2)
```

A.4 Diagonal Spectral Fit Parameter and Abundance Values

Eighteen spectra were extracted and fit with models from the diagonal spectra. Here we present the fit values for all of the models.

A.5 Transverse Spectral Fit Parameter and Abundance Values

Fifteen spectra were extracted and fit with models from the diagonal spectra. Here we present the fit values for all of the models.

Spectra	r^2	$N_H(\frac{atoms}{cm^2})$	kT (keV)	$\tau(\frac{s}{cm^3})$	O ($\odot$)	Ne ($\odot$)	Fe ($\odot$)
1_outrim	0.78	0.04 ± 0.02	1.1 ± 0.3	1.58e+10	0.35 ± 0.5	0.6 ± 0.1	0.31 ± 0.06
2_interest	0.93	0.025 ± 0.02	1.3 ± 0.3	1.92e+10	0.28 ± 0.05	0.5 ± 0.1	0.36 ± 0.8
3_innrim	0.82	0.04 ± 0.02	1.3 ± 0.3	1.23e+10	0.29 ± 0.04	0.56 ± 0.09	0.39 ± 0.07
4	1.27	0.5 ± 0.01	0.7 ± 0.1	3.17e+10	0.2 ± 0.03	0.46 ± 0.06	0.23 ± 0.03
5	1.3	0.05 ± 0.02	0.7 ± 0.1	3.98e+10	0.13 ± 0.02	0.52 ± 0.08	0.22 ± 0.02
6	0.68	0.03 ± 0.02	0.9 ± 0.1	3.81e+10	0.19 ± 0.03	0.7 ± 0.1	0.26 ± 0.06
7	1.1	0.06 ± 0.02	0.9 ± 0.2	2.53e+10	0.25 ± 0.04	0.1 ± 0.1	0.35 ± 0.07
8	1.48	0.06 ± 0.02	0.7 ± 0.1	3.59e+10	0.13 ± 0.02	0.8 ± 0.1	0.47 ± 0.07
9	1.22	0.03 ± 0.01	0.8 ± 0.1	4.82e+10	0.15 ± 0.02	0.49 ± 0.07	0.53 ± 0.07
10	1.13	0.05 ± 0.02	0.9 ± 0.1	3.54e+10	0.13 ± 0.02	0.59 ± 0.09	0.7 ± 0.1
11	1.24	0.03 ± 0.02	1.0 ± 0.1	3.4e+10	0.18 ± 0.03	0.6 ± 0.1	1.0 ± 0.1
12	1.52	0.02 ± 0.02	0.9 ± 0.1	4.72e+1o	1.9 ± 0.03	0.37 ± 0.08	0.8 ± 0.1
13	1.15	0.03 ± 0.02	0.9 ± 0.1	5.37e+10	0.24 ± 0.04	0.44 ± 0.09	0.9 ± 0.1
14	1.07	0.03 ± 0.01	0.8 ± 01	6.94e+10	0.21 ± 0.04	0.24 ± 0.07	0.70 ± 0.09
15	0.96	0.05 ± 0.01	0.8 ± 0.1	4.00e+10	0.14 ± 0.02	0.61 ± 0.08	0.60 ± 0.08
16	1.28	0.01 ± 0.01	0.8 ± 0.01	5.30e+10	0.16 ± 0.02	0.42 ± 0.07	0.71 ± 0.08
17	1.83	0.02 ± 0.01	0.8 ± 0.6	5.29e+10	0.14 ± 0.02	0.57 ± 0.08	0.63 ± 0.08
18	1.58	0.06 ± 0.02	0.74 ± 0.09	4.49e+10	0.10 ± 0.01	0.8 ± 0.1	0.41 ± 0.05

Table A.1: Fit values of timescale parameters and element abundances for diagonal spectral extraction regions.

Spectra	r^2	$N_H(\frac{atoms}{cm^2})$	kT (keV)	$\tau(\frac{s}{cm^3})$	O ($\odot$)	Ne ($\odot$)	Fe ($\odot$)
1t	1.61	0.026 ± 0.006	0.656 ± 0.001	3.00e+10	0.17 ± 0.01	0.37 ± 0.03	0.30 ± 0.02
2t	1.18	0.03 ± 0.01	1.1 ± 0.1	1.07e+10	0.19 ± 0.01	0.43 ± 0.04	0.38 ± 0.03
3t	1.24	0.038	0.82 ± 0.07	5.27e+10	0.10 ± 0.01	0.49 ± 0.06	0.24 ± 0.02
4t	1.00	0.038	0.97 ± 0.09	1.19e+10	0.4 ± 0.1	0.0 ± 0.1	0.98 ± 0.09
5t	0.96	0.038	0.931 ± 0.001	7.30e+10	0.22 ± 0.04	0.2 ± 0.1	1.0 ± 0.1
6t	0.99	0.038	0.813 ± 0.001	8.45e+10	0.23 ± 0.05	0.4 ± 0.1	0.95 ± 0.09
7t	1.16	0.038	1.0 ± 0.1	3.58e+10	0.23 ± 0.03	0.4 ± 0.1	1.2 ± 0.1
8t	1.69	0.02 ± 0.01	0.9 ± 0.1	3.52e+10	0.17 ± 0.02	0.51 ± 0.07	0.7 ± 0.1
9t	1.56	0.02 ± 0.01	0.8 ± 0.1	4.80e+10	0.14 ± 0.02	0.75 ± 0.09	0.64 ± 0.08
10t	1.39	0.038	0.9 ± 0.1	2.96e+10	0.18 ± 0.02	0.85 ± 0.09	0.39 ± 0.04
11t	1.02	0.038	0.55 ± 0.04	7.01e+10	0.16 ± 0.02	0.56 ± 0.07	0.16 ± 0.02
12t	1.09	0.038	0.857 ± 0.007	2.07e+10	0.18 ± 0.01	0.52 ± 0.07	0.28 ± 0.03
13t	1.15	0.038	1.13 ± 0.08	1.38e+10	0.22 ± 0.01	0.0.48 ± 0.04	0.36 ± 0.02
14t	1.32	0.02 ± 0.01	1.0 ± 0.1	1.79e+10	0.25 ± 0.02	0.50 ± 0.05	0.33 ± 0.03
15t	0.84	0.03 ± 0.02	0.7 ± 0.1	2.641e+10	0.30 ± 0.06	0.4 ± 0.1	0.15 ± 0.05

Table A.2: Fit values of timescale parameters and element abundances for transverse spectral extraction regions.

Bibliography

[1] J. Vink. Supernova remnants: the X-ray perspective. *Astronomy and Astrophysics Reviews*, 20:49, December 2012.

[2] S. P. Reynolds. Supernova Remnants at High Energy. *An. Rev. A. A.*, 46:89–126, September 2008.

[3] J. Hong, E. M. Schlegel, and J. E. Grindlay. New Spectral Classification Technique for X-Ray Sources: Quantile Analysis. *ApJ*, 614:508–517, October 2004.

[4] J. Wilms, A. Allen, and R. McCray. On the Absorption of X-Rays in the Interstellar Medium. *ApJ*, 542:914–924, October 2000.

[5] E. Anders and M. Ebihara. Solar-system abundances of the elements. *Geochimica Cosmochimica Acta*, 46:2363–2380, November 1982.

[6] K. A. Frank, V. Dwarkadas, A. Panfichi, R. M. Crum, and D. N. Burrows. Smoothed Particle Inference Analysis of SNR DEM L71. *arXiv e-prints*, March 2019.